JGR Solid Earth

RESEARCH ARTICLE
10.1029/2023JB028013

Improved GRACE-FO Gravity Field Solution by Combining Different Accelerometer Transplant Products

Yufeng Nie[1,2], Yunzhong Shen[1], Jianli Chen[3,4,5], and Qiujie Chen[1]

[1]College of Surveying and Geo-Informatics, Tongji University, Shanghai, China, [2]Now at The Hong Kong Polytechnic University, Hong Kong, China, [3]Department of Land Surveying and Geo-Informatics, The Hong Kong Polytechnic University, Hong Kong, China, [4]Research Institute for Land and Space, The Hong Kong Polytechnic University, Hong Kong, China, [5]Shenzhen Research Institute, The Hong Kong Polytechnic University, Shenzhen, China

Key Points:

- The combination of different ACT products achieves an improved time series of Gravity Recovery and Climate Experiment Follow-on (GRACE-FO) gravity field models with uniformly lower noise levels
- Differences in C_{20} estimates between the combined solution and satellite laser ranging are significantly reduced compared to other GRACE-FO solutions derived from individual ACT products
- Both JPL-ACH and TUG-ACT provide significantly more reliable C_{30} estimates than the JPL-ACT

Supporting Information:

Supporting Information may be found in the online version of this article.

Correspondence to:

Q. Chen,
qiujiechen@tongji.edu.cn

Citation:

Nie, Y., Shen, Y., Chen, J., & Chen, Q. (2024). Improved GRACE-FO gravity field solution by combining different accelerometer transplant products. *Journal of Geophysical Research: Solid Earth*, *129*, e2023JB028013. https://doi.org/10.1029/2023JB028013

Received 5 OCT 2023
Accepted 1 MAY 2024

Author Contributions:

Conceptualization: Yufeng Nie
Data curation: Yufeng Nie
Formal analysis: Yufeng Nie
Funding acquisition: Yunzhong Shen, Qiujie Chen
Investigation: Yufeng Nie, Yunzhong Shen, Jianli Chen, Qiujie Chen
Methodology: Yufeng Nie
Project administration: Qiujie Chen
Resources: Yunzhong Shen, Jianli Chen
Software: Yufeng Nie, Qiujie Chen
Supervision: Yunzhong Shen, Jianli Chen
Validation: Yufeng Nie
Visualization: Yufeng Nie
Writing – original draft: Yufeng Nie
Writing – review & editing: Yufeng Nie, Yunzhong Shen, Jianli Chen, Qiujie Chen

Abstract

Gravity field solutions determined from the Gravity Recovery and Climate Experiment Follow-on (GRACE-FO) are affected by the unexpected performance degradation of one accelerometer onboard, which is circumvented by the accelerometer data transplant (ACT) technique. Three operational ACT products are presently available: JPL-ACT and JPL-ACH from NASA Jet Propulsion Laboratory (JPL) and TUG-ACT from Graz University of Technology (TUG). Considering the heterogeneous qualities of individual ACT products, we propose to combine them to improve the gravity field models after a comprehensive assessment of individual products using a consistent Level-1B data processing. The combination is carried out on the normal equation of gravity field solutions. Spectral, temporal, and spatial evaluations over the period October 2018 to December 2022 demonstrate that the combined solution significantly reduces the noise relative to solutions using individual ACT products, and the average noise reduction rates over JPL-ACT range from 5% to 12% with varying post-processing filters and C_{20} and C_{30} coefficient treatments, which are double those of the second-best JPL-ACH. Moreover, the C_{20} estimate exhibits significant improvement in the combined solution with its deviation from the satellite laser ranging (SLR) solution showing a root mean square (RMS) value of 7.6×10^{-11}, compared to similar RMS values of 15.9×10^{-11}, 12.1×10^{-11}, and 14.9×10^{-11} for JPL-ACT, JPL-ACH, and TUG-ACT, respectively. This improvement helps greatly reduce the amplitude of the 161-day spurious signal over polar regions. For C_{30}, the JPL-ACT gives degraded estimates with an RMS of differences to SLR of 6.2×10^{-11}, while the differences are greatly reduced to 2.6×10^{-11}, 2.7×10^{-11} and 3.6×10^{-11} for the combined solution, JPL-ACH and TUG-ACT, respectively, approaching the formal error of SLR estimates.

Plain Language Summary

The Gravity Recovery and Climate Experiment Follow-on (GRACE-FO) mission continues to provide global measurements of the Earth's gravity field to study large-scale mass redistribution in the Earth system. Monthly snapshots of the Earth's mass changes are routinely provided in terms of gravity field models based on GRACE-FO observation data. However, one accelerometer onboard, used for measuring non-gravitational forces, does not provide the expected high-precision data, which requires the so-called accelerometer data transplant (ACT) technique to copy measurements from the other normally functioning accelerometer. There are currently three operational ACT products but of non-uniform qualities, and, in this study, we combine them to make the best use of each one. Evaluations show that our combined solution achieves consistently lower noise levels than other solutions derived from single ACT products over different months. Moreover, the combined solution offers a significantly improved estimation of C_{20}, the coefficient reflecting the Earth's dynamic oblateness, as validated by the more reliable SLR technique, which is beneficial to the study of mass changes at the largest spatial scale, such as the global mean ocean mass.

1. Introduction

Two decades have passed since the launch of the pioneering twin-satellite mission, the Gravity Recovery and Climate Experiment (GRACE) in 2002, which has revolutionized our way of monitoring global mass changes from seasonal to long-term time scales in the context of global climate change (Tapley et al., 2004, 2019). Based on monthly gravity field models determined from GRACE observations, significant contributions have been made to the quantitative studies of terrestrial water storage variations, global sea level changes, polar ice sheet mass balance, and many others (Cazenave & Chen, 2010; Chen, 2019; Chen et al., 2022; Tapley et al., 2019; Wouters et al., 2014). GRACE was decommissioned in November 2017, and its successor GRACE Follow-On

(GRACE-FO) was successfully launched in May 2018, continuing the global mass change data record from a unique geodetic perspective (Landerer et al., 2020).

The success of GRACE-FO gravity field recovery relies on its high-precision Level-1B (L1B) science data, which mainly consists of inter-satellite measurements provided by both the K/Ka-band microwave instrument (MWI) and the laser ranging interferometer, Global Positioning System data for precise orbit determination, accelerometer (ACC) data recording non-gravitational forces, and satellite attitude data measured by star cameras (SCA) (Landerer et al., 2020). Based on L1B data, monthly gravity field models in the form of unconstrained fully-normalized spherical harmonic (SH) coefficients (and also constrained gridded mascon, but not the focus of this paper) are routinely produced by GRACE-FO Science Data System (SDS), including the Center for Space Research at the University of Texas at Austin (CSR), the NASA Jet Propulsion Laboratory (JPL), and the German Research Center for Geosciences (GFZ). In addition, high-quality gravity field solutions are also provided by various analysis centers (ACs) other than the SDS, such as Graz University of Technology (TUG) (Kvas et al., 2019), Tongji University (Chen et al., 2019; Chen, Shen, et al., 2020), and University of Bern (Meyer et al., 2016), etc. In general, different solutions have quite similar time-varying signal contents, however, their noise levels can differ considerably, even for the SDS solutions using the same L1B data and similar background geophysical models (Chen et al., 2021). The differences mainly come from their specific L1B data processing strategies, in particular their methods of noise modeling as elaborated in Nie et al. (2022a).

One key component of GRACE-FO gravity field recovery involves reducing non-gravitational accelerations (e.g., those caused by atmospheric drag and solar radiation pressure (SRP)) through onboard measurements from two accelerometers. However, starting from 21 June 2018, one of the accelerometers (in GRACE-D) has exhibited significant bias jumps, rendering its data unusable for direct gravity field recovery (Harvey et al., 2022). To address this challenging issue, accelerometer data transplant (ACT) techniques have been developed to "copy" data from the other normal functioning accelerometer, which are based on the assumption that the space environments are quite similar for the two satellites separated by approximately 220 km (Bandikova et al., 2019; Behzadpour et al., 2021; McCullough et al., 2019). Additionally, the quality of ACT products significantly affects the estimation of C_{20} and C_{30} coefficients. These coefficients are crucial in studying mass changes at large spatial scales, such as the global mean ocean mass (GMOM) and the Antarctic ice sheet (Loomis et al., 2019, 2020).

At present, three operational ACT products are available, which are the JPL-ACT and JPL-ACH from JPL, and the TUG-ACT from TUG. In producing JPL-ACT, insights are gained from comparable single-ACC situations in the early and final operational stages of GRACE by implementing sophisticated thruster spike modeling and correction, as well as time and attitude corrections (Bandikova et al., 2019; Harvey et al., 2022; McCullough et al., 2019). Based on JPL-ACT, SDS has produced the Release 6 (RL06) series of gravity field models. Recently, JPL released a new ACT product named JPL-ACH, which hybridizes the real observation data from the GRACE-D accelerometer and the transplanted data (McCullough et al., 2022). As a result, SDS has updated its RL06 solutions to the latest versions, RL06.1 (GFZ and JPL) and RL06.2 (CSR), by substituting JPL-ACT with JPL-ACH during L1B data processing (Flechtner et al., 2023). In a parallel development, TUG offers an alternative ACT product, where a novel remove-restore technique is introduced by first removing a major portion of non-gravitational forces via the use of empirical models and then carrying out the data transplant at the residual level (Behzadpour et al., 2021).

The quality of different ACT products has an important impact on the solved gravity field solutions. Behzadpour et al. (2021) demonstrated that gravity field models derived from TUG-ACT have lower noise levels than those from JPL-ACT. Additionally, the corresponding C_{20} and C_{30} coefficients are more consistent with those estimated from SLR data. Ghobadi-Far et al. (2023) found that JPL-ACH leads to significantly improved C_{30} estimates and consistently reduces solution noise compared to its predecessor, JPL-ACT, through systematic comparisons between the SDS RL06 and RL06.1 solutions. However, independent assessments of all three operational ACT products are still lacking in the current literature, which will require consistent L1B data processing to give fair and meaningful results. This is one of the motivations for this study.

The other motivation arises from the above evaluation process that reveals heterogeneous performances of individual ACT products across different months, that is, a specific ACT product is not necessarily always the best (see Figure 4). Therefore, we propose to optimally combine gravity field solutions derived from different ACT products to reduce their individual errors in non-gravitational force modeling, which is expected to generate an improved model series with consistently lowered noise levels. This is also the philosophy behind many geodetic solution combination campaigns. For example, the International GNSS Service integrates orbit solutions from different ACs to provide the most precise products (Dow et al., 2009); the International Combination Service for Time-variable Gravity Fields (COST-G) aims at delivering best-quality global gravity field model by incorporating contributions from several GRACE/GRACE-FO ACs worldwide (Jäggi et al., 2019, 2020).

This paper is structured as follows: Section 2 details our L1B data processing strategies for GRACE-FO gravity field recovery. Moreover, we present the ACT product combination method via normal equations of gravity field solutions and the descriptions of two corresponding weighting schemes. Section 3 examines the impacts of different weightings on the combined solution, followed by comprehensive evaluations of individual single-ACT solutions and the combined solution in spectral, temporal, and spatial domains. Furthermore, we evaluate the quality of C_{20} and C_{30} estimates using SLR-derived values as the references. Finally, Section 4 outlines conclusions and discusses future research possibilities.

2. Data and Methods

2.1. Gravity Field Recovery From L1B Data

We use the classical dynamic approach for gravity field recovery, which links GRACE-FO observations to gravity field parameters by numerically integrating the satellite's equations of motion and the variational equations (Bettadpur & McCullough, 2017; Reigber, 1989). During the orbit integration, a suite of background dynamic and geophysical models is utilized to reduce signals stemming from static gravity field, tides, and non-tidal atmospheric and oceanic variations, all of which are outlined in Table 1. The RL06 of the Atmosphere and Ocean De-Aliasing Level-1B (AOD1B) product is adopted to be consistent with the SDS RL06 and RL06.1 solutions (Dobslaw et al., 2017). The version 04 L1B data from JPL and kinematic orbits from TUG (Suesser-Rechberger et al., 2022; Zehentner & Mayer-Gürr, 2015) are utilized to generate three sets of monthly gravity field model series from October 2018 to December 2022 using JPL-ACT, JPL-ACH, and TUG-ACT respectively via consistent L1B data processing.

The parameter estimation process involves two steps: orbit fitting and gravity recovery (Tapley et al., 2005). Satellite initial states of each 6-hr orbit arc, accelerometer bias, and scale calibration parameters are estimated in the orbit fitting step. In the gravity recovery step, these parameters are re-estimated along with gravity field parameters in the form of fully-normalized SH coefficients up to degree and order (d/o) 96. The range rates from MWI, consistent with SDS solutions, and kinematic orbit positions are used in the above steps. The accelerometer bias is modeled as a third-order polynomial to account for its temporal variations and is estimated once per day, while a fully-populated accelerometer scale matrix is estimated monthly to consider the cross-talk and misalignment in the accelerometer frame (Chen et al., 2019; Klinger & Mayer-Gürr, 2016). Instead of estimating empirical parameters, either in the form of accelerations or range-rate parameters, stochastic modeling is employed (Nie et al., 2022a). In stochastic modeling, an autoregressive model-based filtering approach is adopted to properly model colored noise in the data during the weighted least-squares parameter estimation process, detailed in Nie et al. (2022a). Additionally, relative weights between different observation groups are determined based on the variance component estimation (VCE) (Koch & Kusche, 2002; Kusche, 2003), which is realized by an efficient algorithm developed by Nie, Shen, Pail, and Chen (2022).

2.2. ACT Product Combination

We combine different ACT products based on normal equations (NEQ) of gravity field solutions derived from the individuals. The combination is carried out at the level of NEQ instead of SH coefficients to fully consider correlations among parameters (Meyer et al., 2019), which reads

$$\left(\sum_{i=1}^{3} w_i \boldsymbol{N}_i\right)\hat{\boldsymbol{x}} = \left(\sum_{i=1}^{3} w_i \boldsymbol{b}_i\right) \tag{1}$$

where $\hat{\boldsymbol{x}}$ is the vector of gravity field parameters to be estimated, $\boldsymbol{N}_i$ and $\boldsymbol{b}_i$ are normal matrix and right-hand-side vector of NEQ, the construction of which is detailed in Nie et al. (2022a, 2022b). Three groups of NEQ are derived from JPL-ACT, JPL-ACH, and TUG-ACT, respectively, and they are weighted based on corresponding

10.1029/2023JB028013

Table 1
Background Dynamic and Geophysical Models Used in GRACE-FO Gravity Field Recovery

Background models	Description
Static gravity field	GOCO06s (Kvas et al., 2021) with degree and order (d/o) 160
N-body perturbations	JPL DE440 (Park et al., 2021)
Solid Earth tides	IERS 2010 convention (Petit & Luzum, 2010)
Solid Earth pole tides	IERS 2010 convention
Ocean tides	EOT11a (Savcenko & Bosch, 2012) with d/o 120
Ocean pole tides	IERS 2010 convention (Desai, 2002) with d/o 120
Non-tidal de-aliasing	AOD1B RL06 (Dobslaw et al., 2017) with d/o 120
Atmospheric tides	AOD1B RL06 with d/o 120
General relativistic corrections	IERS 2010 convention
Non-gravitational forces	JPL-ACT, JPL-ACH and TUG-ACT

factors w_i. Two weighting schemes are introduced in this paper, one is based on VCE, and the other on empirical noise estimation.

By VCE, the weight factor is derived as

$$w_i = \frac{n_i - t_i}{\hat{\boldsymbol{x}}^T \boldsymbol{N}_i \hat{\boldsymbol{x}} - 2\hat{\boldsymbol{x}}^T \boldsymbol{b}_i + \boldsymbol{l}_i^T \boldsymbol{P}_i \boldsymbol{l}_i} \tag{2}$$

where $(\cdot)^T$ denotes the transpose operator, $\boldsymbol{l}_i$ is the reduced observation data vector, and $\boldsymbol{P}_i$ is the weight matrix determined from the filtering approach in this study (Nie et al., 2022a); n_i is the number of observations reduced by local parameters, for example, initial states and accelerometer calibration parameters, and t_i is contribution number of each solution to the joint estimation of $\hat{\boldsymbol{x}}$, which is computed as (Nie, Shen, Pail, & Chen, 2022)

$$t_i = \mathrm{tr}\left(w_i \boldsymbol{N}_i \left(\sum_{i=1}^{3} w_i \boldsymbol{N}_i \right)^{-1} \right) \tag{3}$$

where $\mathrm{tr}(\cdot)$ denotes the trace operator of a matrix. The VCE is performed iteratively and starts with equal weights, that is, $w_1 = w_2 = w_3 = 1.0$.

For the empirical noise estimation-based weighting scheme, we use the open ocean residuals (OOR) to represent the noise level of different solutions, which is the most commonly used metric in GRACE/GRACE-FO model assessments (Chen et al., 2019, 2021; Kvas et al., 2019; Meyer et al., 2016). Here, the open ocean is defined as oceanic areas more than 500 km away from the coastlines (Chen et al., 2021). For a specific set of model time series, the ORR is derived as follows: we first convert SH coefficients, after subtracting a static or mean model, to gridded values of equivalent water height (EWH) (Wahr et al., 1998), then use unweighted least squares to fit and remove a climatology model, made up by bias, trend, annual and semi-annual sinusoids, from the EWH time series of each grid over the available GRACE-FO period, which gives the grid-wise residuals; by calculating the root mean square (RMS) value of residuals from all grids within the open ocean, we get the empirical estimation of model noise σ_i, or what we abbreviate as OOR RMS in the following, with

$$\sigma_i = \sqrt{\frac{\sum_{j\in\Omega} \cos(\varphi_j) \Delta h_j^2}{\sum_{j\in\Omega} \cos(\varphi_j)}} \tag{4}$$

where Δh_j is the residual EWH of grid j with the latitude of φ_j; the scale $\cos(\varphi_j)$ is introduced to consider the varying grid sizes at different latitudes and Ω represents the open ocean. As a major part of time-variable signals are already removed by the AOD1B product and ocean tide model during the L1B data processing, the remaining non-steric signals over open oceans can be reasonably well modeled by the above simple climatology model

(Chen et al., 2021). Therefore, OOR is dominated by noise, and its RMS value σ_i can be regarded as a proxy of the upper bound of the solution noise level. Accordingly, the weight factor is simply the inverse of the squared noise level as $w_i = 1/\sigma_i^2$.

3. Results and Analysis

3.1. Combined Solutions With Different Weighting Schemes

For the empirical noise estimation-based weighting, a 300-km Gaussian smoothing is applied (Wahr et al., 1998), otherwise, the estimated noise level will solely reflect the highest SH degrees (Kvas et al., 2019). The Glacial Isostatic Adjustment (GIA) effect, degree-0 and degree-1 coefficients are not considered as they have a common impact on all individual solution noise estimates, while for the combination only relative weights matter. Moreover, the C_{20} and C_{30} are deliberately not replaced by SLR-derived values in Technical Note TN-14 (Loomis et al., 2019, 2020), because their uncertainties are naturally part of the noise budget, and are what we would like to address with different ACT products.

Figures 1a and 1b show monthly normalized weights of solutions derived from JPL-ACH and TUG-ACT with respect to JPL-ACT based on VCE and empirical noise estimation (denoted as EMP in the figure), respectively. In general, weights of different ACT products are comparable in both cases, while those derived from empirical noise estimation show larger fluctuations with the JPL-ACH getting the largest weights. The relatively consistent weights, that is, close to 1.0, estimated in the VCE case are within our expectation, because we have applied stochastic modeling in the construction of individual NEQ, which already takes into account data heterogeneity via fully-populated observation weight matrices (Brockmann et al., 2021; Nie et al., 2022a). Moreover, as VCE is mainly driven by the internal (or formal) precision of the parameter estimation system, any deviation from the truth in stochastic modeling cannot be self-calibrated (Lerch, 1991). This holds for our current study because error information of background geophysical models, for example, ocean tide model and AOD product, has not been fully considered (Abrykosov et al., 2022; Kvas & Mayer-Gürr, 2019). This also partially explains the non-uniform, yet potentially more realistic, weights determined by the empirical noise estimation. Nevertheless, no distinct difference can be observed between the two combined solutions, as reflected in the OOR RMS time series after 300-km Gaussian smoothing in Figure 1c. Therefore, we use the empirical noise estimation in the following to weigh different ACT products due to its ease of implementation.

3.2. Evaluations of the Combined Solution

In this section, we comprehensively evaluate three individual gravity field solutions, denoted as JPL-ACT, JPL-ACH, and TUG-ACT, for compactness, generated by the corresponding ACT product, and the thereof combined solution, denoted as COMB hereafter, in spectral, temporal, and spatial domains.

Figure 2 shows the average geoid heights from October 2018 to December 2022 of the four solutions with respect to the static gravity field model GOCO06s, in degree-wise (Figure 2a) and order-wise (Figure 2b) manner. In the degree-wise plot, the four solutions are almost identical for degrees below 30 (except for degrees 2 and 3 to be discussed in Section 3.3), indicating that they capture consistent time-varying gravity signals characterized by decreasing energy at shorter wavelengths. At higher degrees, the geoid height steadily increases and is dominated by noise due to the nature of satellite gravity inversion, a typical ill-posed problem where noise is amplified at the high-frequency bands (Save et al., 2012). In the mid- and high-frequency bands, COMB has the lowest noise level, while JPL-ACT has the highest; JPL-ACH outperforms TUG-ACT on average, especially for degrees between 45 and 55. The order-wise plot shows similar results, with the combined solution giving less noise than the other three for higher-order SH coefficients. In addition, distinct peaks appear at SH orders of multiples of ∼15 due to the well-understood orbital resonance effect, where the combined solution is the least contaminated.

We further investigate two special groups of SH coefficients, the sectorial and the zonal coefficients, as shown in Figures 3a and 3b, respectively. The sectorial coefficients are known to be prone to errors in dynamic force models (Beutler et al., 2010), hence the generally lower noise levels of JPL-ACH and TUG-ACT than JPL-ACT in this frequency band indicate better modeling of non-gravitational forces. Combining the three enables further noise reduction, which takes advantage of individual ACT techniques. For zonal coefficients, however, we cannot tell any difference among solutions except for C_{20} and C_{30}, indicating a smaller impact of the different ACT products on this spectral group.

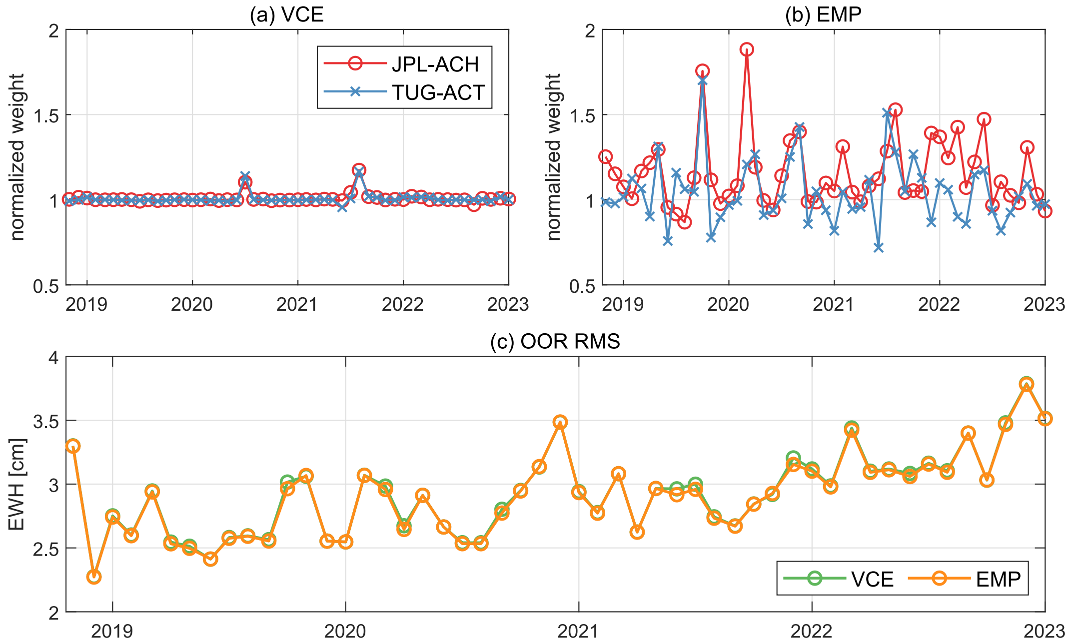

Figure 1. (a) Normalized weights of JPL-ACH and TUG-ACT with respect to JPL-ACT in solution combination determined by variance component estimation. (b) same as panel (a) but determined by empirical noise estimation (EMP). (c) Monthly open ocean residuals root mean square (RMS) values of the two combined solutions with 300-km Gaussian smoothing applied.

In the temporal domain, monthly OOR RMS values after 300-km Gaussian smoothing are shown in Figure 4. Heterogeneous noise levels among the different ACT products and the non-uniform performance of individuals over time are clearly presented. In general, improvements of JPL-ACH over its predecessor JPL-ACT are apparent, consistent with the results of Ghobadi-Far et al. (2023), while the combined solution has the lowest noise level for most of the months. When C_{20} and C_{30} coefficients are excluded, as shown in Figure 4b, OOR become slightly smaller and closer among different solutions. Besides, we also observe a systematic increase in noise for all solutions starting in 2021, mainly due to the build-up of the 25th solar cycle (Landerer et al., 2022). The National Oceanic and Atmospheric Administration (NOAA) total solar irradiance time series (Coddington

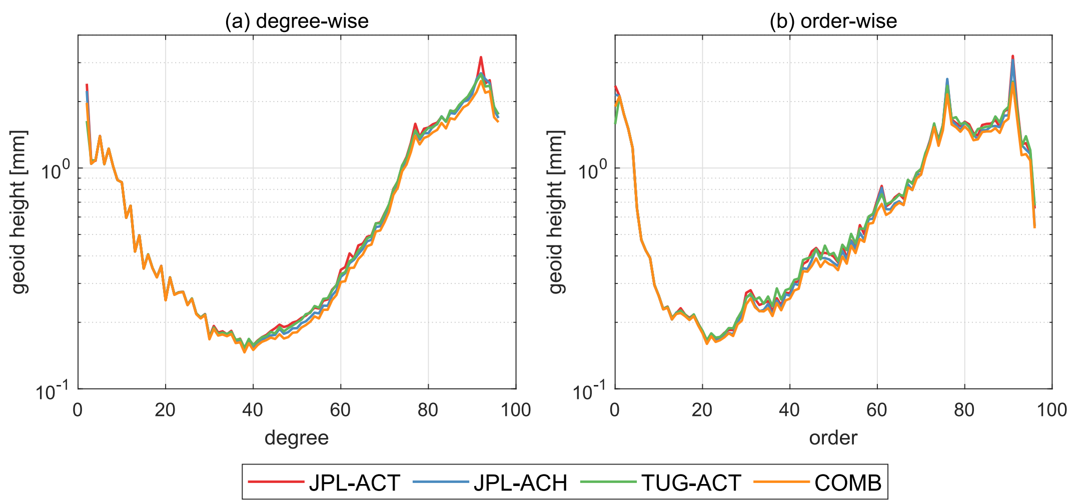

Figure 2. Average geoid heights from October 2018 to December 2022 of four solutions with respect to GOCO06s. (a) for degree-wise plot, (b) for order-wise plot.

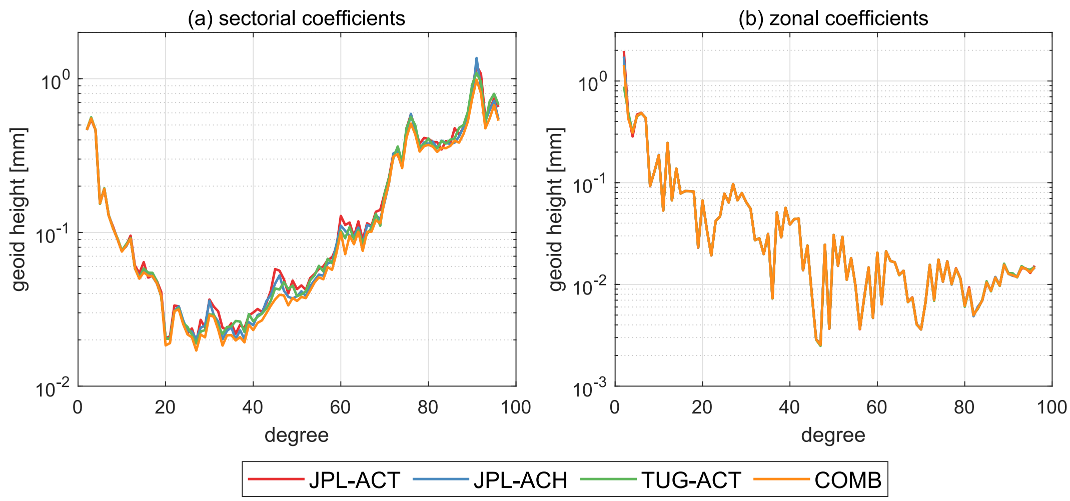

Figure 3. Degree-wise average geoid heights from October 2018 to December 2022 of four solutions with respect to GOCO06s. (a) for sectorial coefficients only, (b) for zonal coefficients only.

et al., 2016), shown as the gray curve in Figure 4, reflects the intensification of solar activity after 2021, which leads to stronger non-gravitational forces and thus challenges the technique of ACT.

Figure 5 demonstrates the relative noise reduction rates of JPL-ACH, TUG-ACT, and COMB with respect to JPL-ACT based on the results in Figure 4a. As expected, the combined solution achieves the greatest noise reduction for almost all months, while there are several months where TUG-ACT shows larger noise than JPL-ACT and a few months where JPL-ACH gives negative values. We also plot the β' angle, defined as the angle between the Earth-satellite plane and the Earth-Sun plane, in Figure 5 to show the evolution of the improvements with it, which varies between -90 and $90°$ with a period of approximately 161 days. From a visual inspection, the largest noise reduction

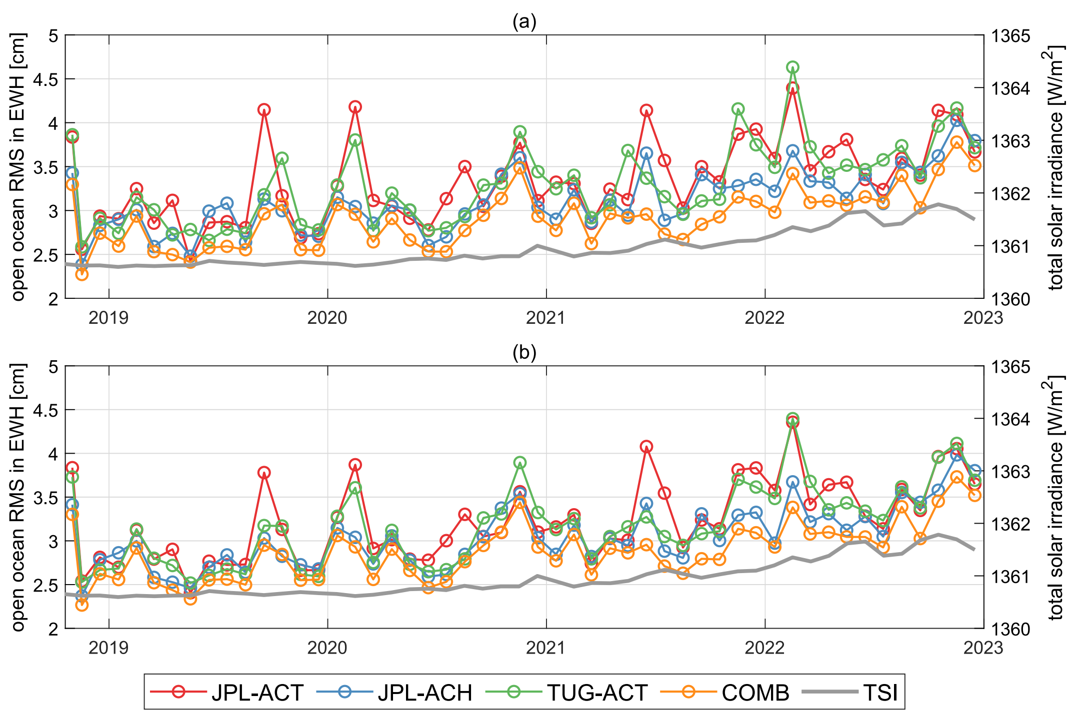

Figure 4. Monthly open ocean residuals root mean square (RMS) values of four solutions. C_{20} and C_{30} coefficients are included in panel (a) and excluded in panel (b). 300-km Gaussian smoothing is applied. The gray curve represents the total solar irradiance.

10.1029/2023JB028013

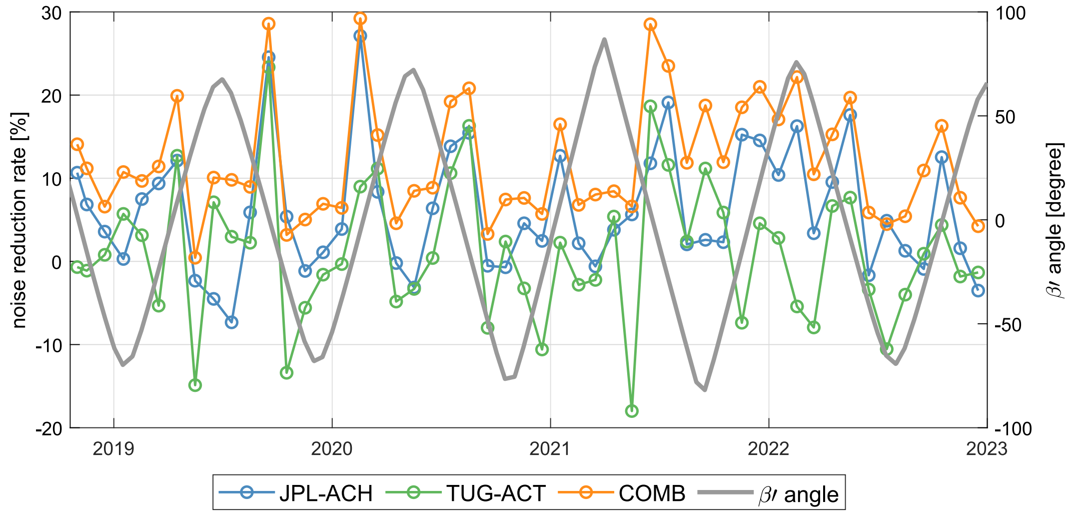

Figure 5. Monthly noise reduction rates of JPL-ACH, TUG-ACT, and COMB over JPL-ACT based on noise estimates in Figure 4a. The gray curve represents the β' angle.

is achieved when β' is close to zero, as pointed out by Ghobadi-Far et al. (2023). Furthermore, we present the noise reduction rates of each month with respect to the corresponding β' angles in Figure 6. Specifically, Figure 6a is based on the results of Figure 5, while Figure 6b additionally replaces C_{20} and C_{30} with SLR estimates. Both cases demonstrate that the largest improvements over JPL-ACT are indeed clustered around the zero β' angle (with a few exceptions). To gain more insight into the β' dependency, we compare the L1B acceleration data of three ACT products by setting the state-of-the-art JPL-ACH as the reference. The time series of differences for JPL-ACT and TUG-ACT (both with respect to JPL-ACH) are zero-centered on a daily basis to account for their different accelerometer bias treatments during the transplant (Behzadpour et al., 2021; Harvey et al., 2022). Figure 7 displays the daily RMS values for each acceleration component, along with the β' angles. It clearly demonstrates that the largest along-track and radial acceleration differences occur near zero β'. During this period, satellites undergo significant temperature fluctuations, resulting in substantial variations in non-gravitational forces, particularly SRP, and therefore challenging the accelerometer data transplant (Behzadpour et al., 2021; Cheng & Ries, 2017; Ghobadi-Far et al., 2023; Harvey et al., 2022; Klinger & Mayer-Gürr, 2016). This largely explains why the most noticeable improvements or degradations in gravity field solutions using different ACT products are observed with zero β'. In the cross-track direction, the differences between TUG-ACT and JPL-ACH are about two orders of magnitude larger than those between the two JPL products. This could be caused by SRP mismodeling and/or the

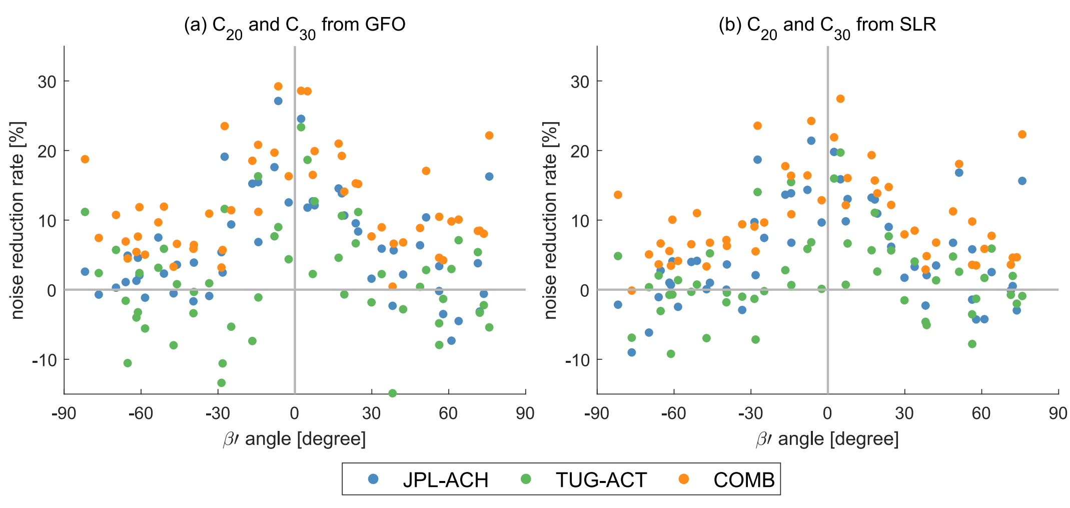

Figure 6. (a) Noise reduction rates in Figure 5 in terms of β' angle. (b) same as panel (a) but with C_{20} and C_{30} replaced by satellite laser ranging estimates.

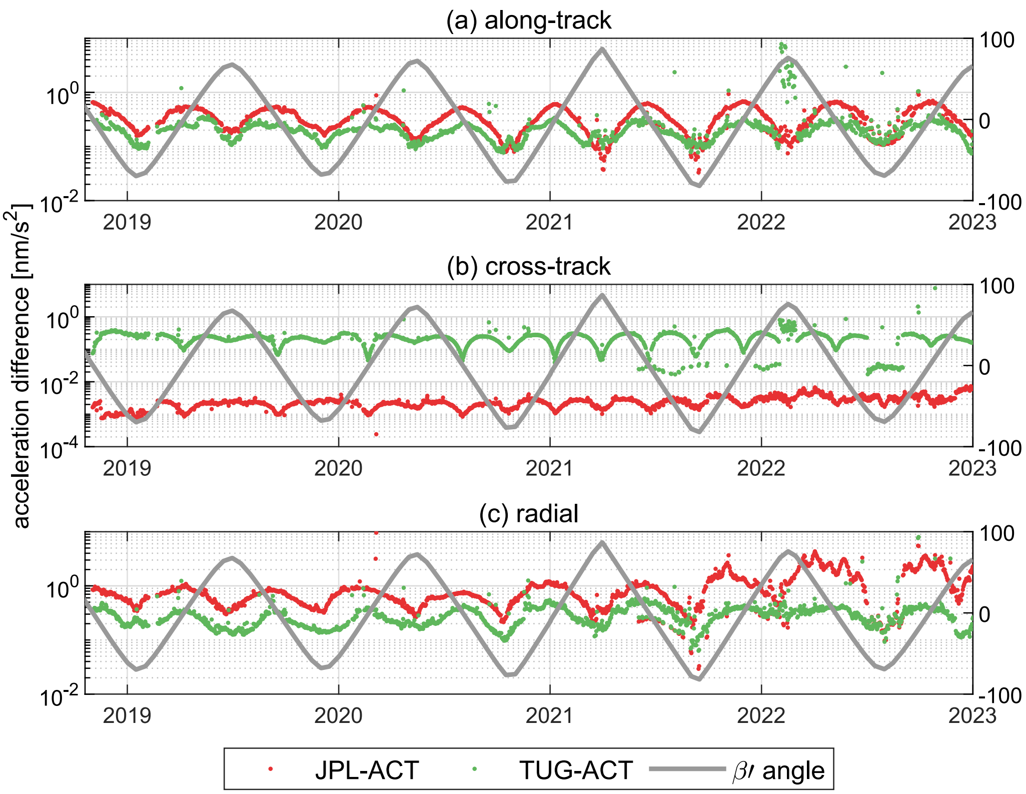

Figure 7. Daily root mean square (RMS) values of acceleration differences of JPL-ACT and TUG-ACT with respect to JPL-ACH in along-track (a), cross-track (b), and radial (c) directions.

pitch offset, but further investigation is needed (Behzadpour et al., 2021; Harvey et al., 2022). Nevertheless, these systematic cross-track deviations are expected to have minor impacts on gravity field solutions due to the co-estimation of accelerometer calibration parameters and the along-track dominated observation pattern of GRACE-FO (Harvey et al., 2022). Additionally, Figure 7 illustrates that JPL-ACT deviates from JPL-ACH more and more after 2021 as a result of increased solar activities, which is exemplified in Figure S1 in Supporting Information S1 for two randomly selected days in 2019 and 2022.

Table 2 summarizes the average noise reduction rates of all months for individual gravity field solutions with different post-processing filters and treatments of C_{20} and C_{30}. In addition to the 300-km Gaussian smoothing (denoted as G300), the decorrelation filter (denoted as DC) proposed by Swenson and Wahr (2006) and modified by Chen et al. (2010) is utilized to suppress the stripe noise, where fourth-order polynomials are fitted to remove correlations among the odd (and even) order SH coefficients starting from degree 6. In the various cases in Table 2, the average noise reduction rates of JPL-ACH over JPL-ACT are between 2% and 7%, while those of the COMB are twice as high, indicating that combining different ACT products can bring significantly more benefits than using the up-to-date JPL-ACH alone. When using G300 alone, an average noise reduction of 10% or 12% is achieved, regardless of whether C_{20} and C_{30} are replaced by SLR estimates or not. For TUG-ACT, the noise reduction rates are minor on average when assessed with the G300 filter, and are even negative when both DC and G300 filters are applied. This can be a result of its heterogeneous noise behavior, based on our L1B data processing strategy, across different months and hence canceling out positive and negative values on average (see Figure 5), which justifies the motivation to combine different ACT products to provide consistently better monthly model series.

Table 2
Mean Noise Reduction Rates (Unit: %) of Months From October 2018 to December 2022 of JPL-ACH, TUG-ACT, and COMB Over JPL-ACT Assessed by Different Post-Processing Filters and Treatments of C_{20} and C_{30}

		JPL-ACH	TUG-ACT	COMB
G300	GFO C_{20}/C_{30}	6.1	1.1	12.0
	SLR C_{20}/C_{30}	5.3	1.8	10.4
DC + G300	GFO C_{20}/C_{30}	4.7	−1.7	9.7
	SLR C_{20}/C_{30}	2.4	−0.2	5.1

Note. G300 denotes the 300-km Gaussian smoothing, and DC denotes the decorrelation filter.

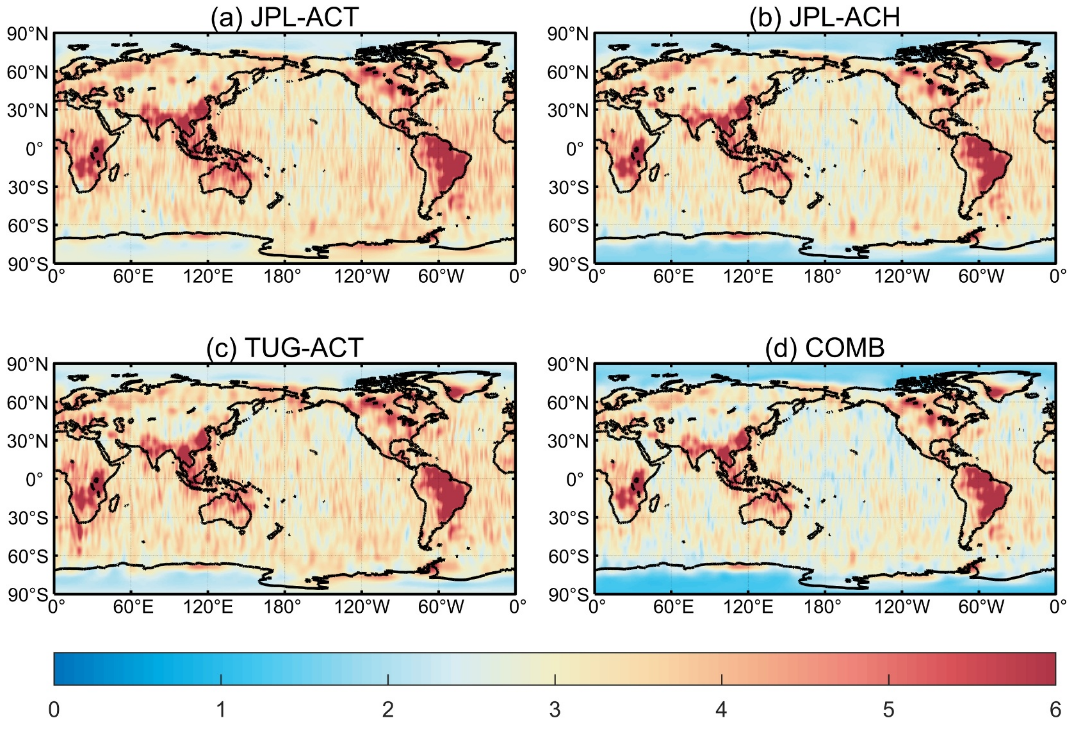

Figure 8. Spatial distribution of noise in four solutions (unit: cm). 300-km Gaussian smoothing is applied, and C_{20} and C_{30} are from Gravity Recovery and Climate Experiment Follow-on estimates.

Figure 8 further illustrates the spatial distribution of noise in different solutions, derived by taking the (temporal) RMS of the monthly residual EWH for each grid (Chen et al., 2021). We can observe some large RMS values over land, mainly due to intra-seasonal and possibly interannual signals not well captured by the simple climatology model (Chen et al., 2021). In the open ocean, JPL-ACH has systematically less noise than JPL-ACT and TUG-ACT, both in spatial extent and intensity, while COMB reduces it even further. Furthermore, JPL-ACH and COMB show smaller values over polar regions than the other two, mainly due to their different C_{20} and C_{30} estimates. By replacing them with SLR-derived values, four solutions are more consistent in polar regions (not shown).

Finally, for external validation, we compare our combined solution (COMB) with the latest SDS solutions from JPL (RL06.1), GFZ (RL06.1) and CSR (RL06.2). Figure 9 shows the degree-wise mean geoid heights of the individual solutions, which are consistent in low degrees, while our solution shows remarkably lower noise, especially in higher degrees. We attribute this to the employed stochastic modeling (Nie et al., 2022a, 2022b) and to the combination of different ACT products. Figure 10 shows the noise estimates of each monthly solution, with C_{20} and C_{30} replaced by SLR-derived values and both DC and G300 filters applied. It indicates that the COMB consistently achieves the lowest noise level. Besides, among the three SDS solutions, CSR generally shows superior performance and is closely followed by JPL. To guarantee that the lower noise level of COMB does not come at the expense of signal distortion, we estimate trends and annual amplitudes of 123 river basins (Scanlon et al., 2016), with an area larger than 100,000 km^2, for the four solution time series. Figure 11 shows the COMB estimates compared to the reference SDS estimates, which are defined as the average of JPL, GFZ, and CSR. The values of COMB are linearly regressed against SDS, following the methodology of Scanlon et al. (2016). The fitted slopes for trend and annual amplitude are 1.00 and 0.98, respectively, confirming their consistent signal contents. Figure S2 in Supporting Information S1 displays the EWH change time series for the Antarctic and Greenland ice sheets, as well as some selected river basins, with GIA signals removed by the ICE6G-D model (Peltier et al., 2018).

3.3. Impacts on C_{20} and C_{30} Coefficients

Since non-gravitational forces exhibit distinct once-per-revolution and twice-per-revolution features in orbit perturbations (Beutler et al., 2006; Scharroo & Visser, 1998), improvements in the ACT product or treatment are

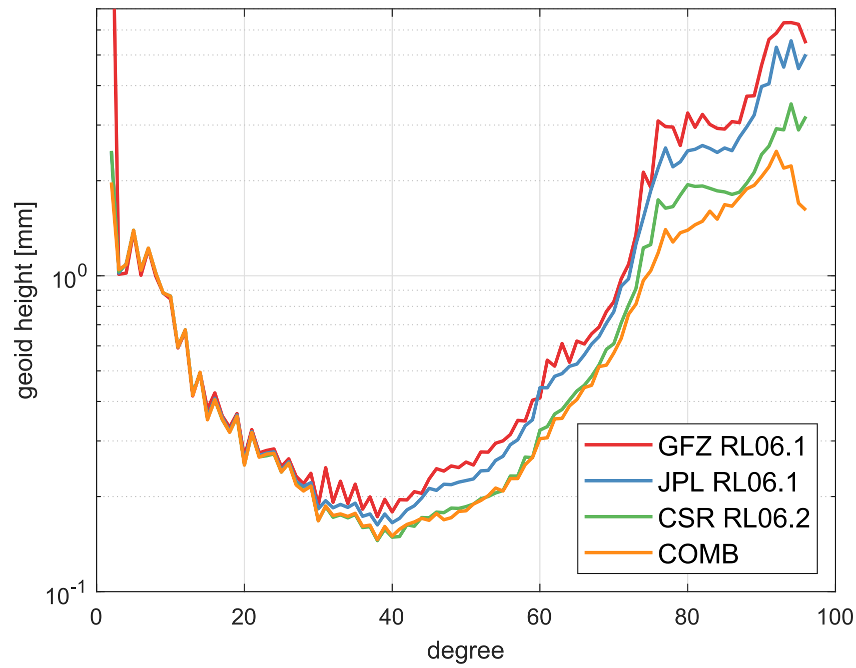

Figure 9. Degree-wise mean geoid heights with respect to GOCO06s of the combined solution from this study (COMB) and three SDS solutions (CSR/JPL/GFZ) averaged over months from October 2018 to December 2022.

expected to refine the C_{20} estimate of GRACE-FO. In addition, recent investigations by Loomis et al. (2020) have shown that the quality of the C_{30} estimate based on JPL-ACT is degraded and recommended replacing it with the SLR-derived one. Therefore, in the following we assess the impact of updated ACT products and their combination on these two coefficients.

Figure 12 shows the time series of C_{20} estimates from individual gravity field solutions using different ACT products and from the combined solution. The SLR-derived values provided in TN-14 are plotted for reference as they are believed to be more reliable. As indicated, JPL-ACH shows improvements over JPL-ACT and TUG-ACT for generally reduced discrepancies with SLR. The RMS of its differences to SLR is 12.1×10^{-11}, while

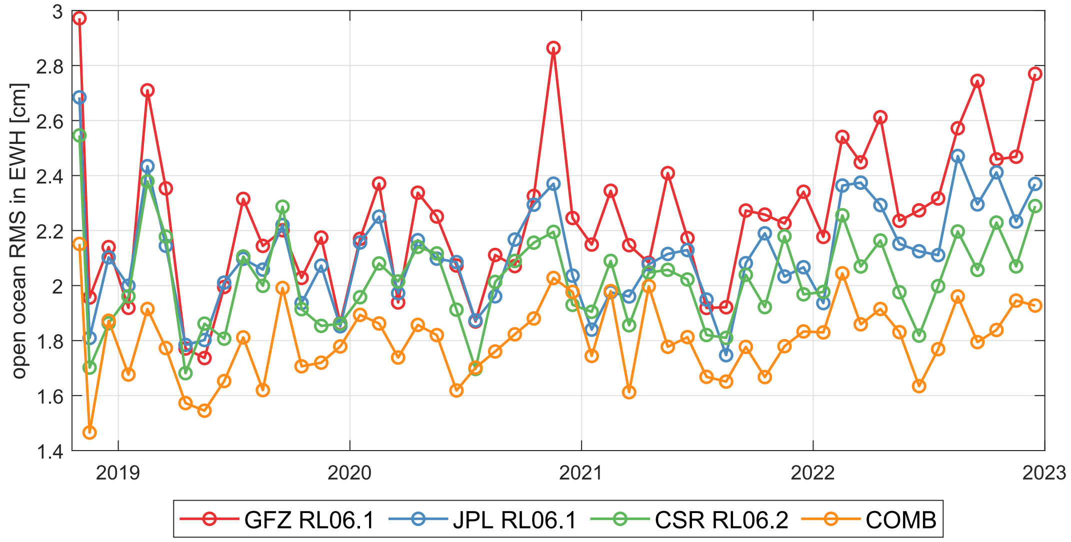

Figure 10. Monthly open ocean residuals root mean square (RMS) values of four solutions. Decorrelation filter and 300-km Gaussian smoothing are applied, and C_{20} and C_{30} are replaced by satellite laser ranging estimates.

10.1029/2023JB028013

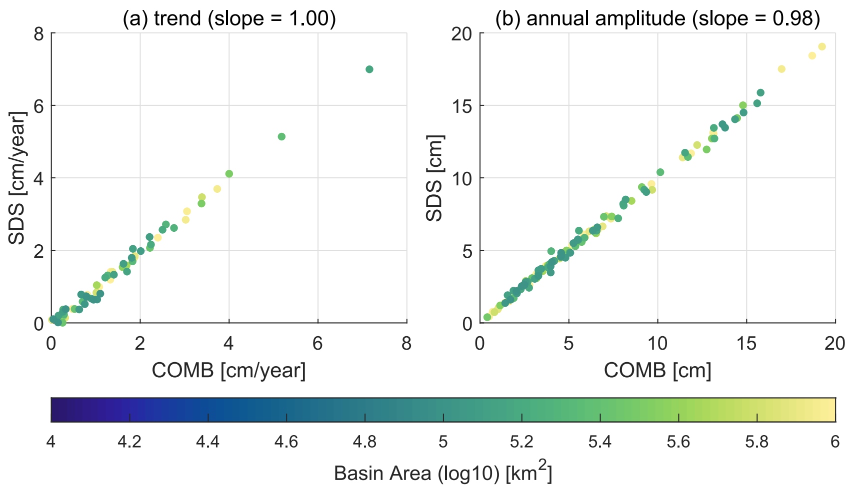

Figure 11. Estimates of trend (a) and annual amplitude (b) of 123 river basins. The SDS value represents the average of CSR, JPL, and GFZ estimates. Slopes are fitted based on the displayed COMB and SDS values using least squares. Decorrelation filter and 300-km Gaussian smoothing are applied, and C_{20} and C_{30} are replaced by satellite laser ranging estimates.

it is 15.9×10^{-11} and 14.9×10^{-11} for JPL-ACT and TUG-ACT, respectively, as summarized in Table 3. By combining different ACT products, the COMB further reduces the RMS value to 7.6×10^{-11}, which is only half that of JPL-ACT and significantly smaller than the state-of-the-art JPL-ACH, given the formal error of the SLR estimates in TN-14 is about 2×10^{-11}.

Figure 13 shows the results of C_{30}. Both JPL-ACH and TUG-ACT give significantly more reliable estimates than JPL-ACT, as reported in Behzadpour et al. (2021) and Ghobadi-Far et al. (2023). Among the four, JPL-ACH and COMB come closest to the SLR with RMS values less than 3×10^{-11} in Table 3, which is at the same level as the C_{30} formal error of the SLR. This brings us to the consideration of whether it is still necessary to replace GRACE-FO C_{30} with SLR for JPL-ACH or COMB, but this is beyond the scope of the present study. Moreover, when presenting the absolute differences of C_{30} between GRACE-FO and SLR in terms of β' angles, Figure 14 reveals that their dependencies on β' are significantly reduced in JPL-ACH, TUG-ACT and COMB, compared to JPL-ACT, which further indicates improvements in C_{30} estimates with the updated ACT products and treatments.

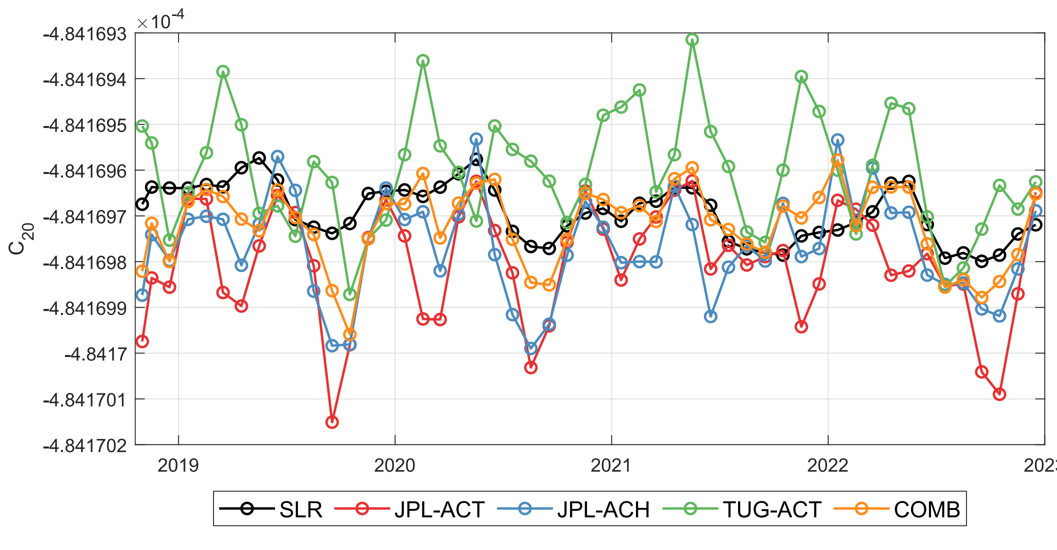

Figure 12. C_{20} estimates of Gravity Recovery and Climate Experiment Follow-on in four gravity field solutions. The satellite laser ranging values are given for reference.

Table 3
Root Mean Square (RMS) Values of Differences in C_{20} and C_{30} Estimates Between Four GRACE-FO Solutions and the SLR

($\times 10^{-11}$)	JPL-ACT	JPL-ACH	TUG-ACT	COMB
C_{20}	15.9	12.1	14.9	7.6
C_{30}	6.2	2.7	3.6	2.6

To investigate what the improvements in C_{20} and C_{30} estimates can bring about, we fit the 161-day sinusoids (along with bias, trend, annual, and semi-annual terms) for each grid of the four solutions and plot the grid-wise amplitudes in Figure 15. C_{20} and C_{30} are kept as GRACE-FO estimates, and a 300-km Gaussian smoothing is applied. The non-geophysical 161-day signal is a known issue in GRACE/GRACE-FO gravity field solutions, the origin of which has been commonly assumed to be the S2 ocean tide aliasing (Chen et al., 2008; Han et al., 2005; Seo et al., 2008), while recent studies suggest a close relationship with accelerometer errors caused by the 161-day angular evolution of β' (Cheng & Ries, 2017; Klinger & Mayer-Gürr, 2016). Figure 15 shows that the amplitudes in the Antarctic are quite large for JPL-ACT and TUG-ACT, while they are considerably attenuated for JPL-ACH and especially COMB. They also show a latitudinal dependence, thus we compute the average amplitude of each latitudinal band and plot it in Figure 16a along with the corresponding latitudes. It is clearly shown that COMB has the least latitude dependence, and the latitudinal average amplitudes of JPL-ACT and TUG-ACT are larger than those of JPL-ACH and COMB. To understand which factor contributes to the above results, C_{30} is replaced with SLR-derived value in Figure 16b, but the results remain basically the same. When both C_{20} and C_{30} are replaced, Figure 16c shows that the four solutions now obtain consistent and insignificant 161-day amplitudes in all latitude bands. This confirms that the greatly reduced artificial signals in JPL-ACH and COMB are attributed to their improved estimation of C_{20}. Moreover, our preliminary results support the speculation that the 161-day signal is highly associated with the accelerometer errors since we use the same ocean tide model in producing the four solutions. Nevertheless, further investigation with a longer time series is needed to address this open issue fully.

To evaluate the effect of C_{20} and C_{30} improvements on mass change study, we use GMOM as a demonstration example. We estimate the time series of GMOM changes in terms of EWH using the four gravity field solutions mentioned above. After GIA correction using the ICE6G-D model, the solutions are smoothed with a 300-km Gaussian filter, and an ocean mask with a 500-km buffer zone is applied to reduce leakage error (Chen, Tapley, et al., 2020). C_{20} and C_{30} coefficients are kept as their own estimates by GRACE-FO to focus on their direct impacts. The results are compared to the reference, which is defined as an ensemble mean of three SDS solutions with C_{20} and C_{30} replaced by SLR estimates as recommended by Loomis et al. (2019, 2020). Figure 17 shows the differences with respect to the reference. JPL-ACT and TUG-ACT deviate up to 5 mm from the reference, while JPL-ACH and COMB have the smallest deviations, which aligns with the evaluations on C_{20} and C_{30} in Table 3. However, when both C_{20} and C_{30} are replaced with SLR estimates, the four GMOM change time series become

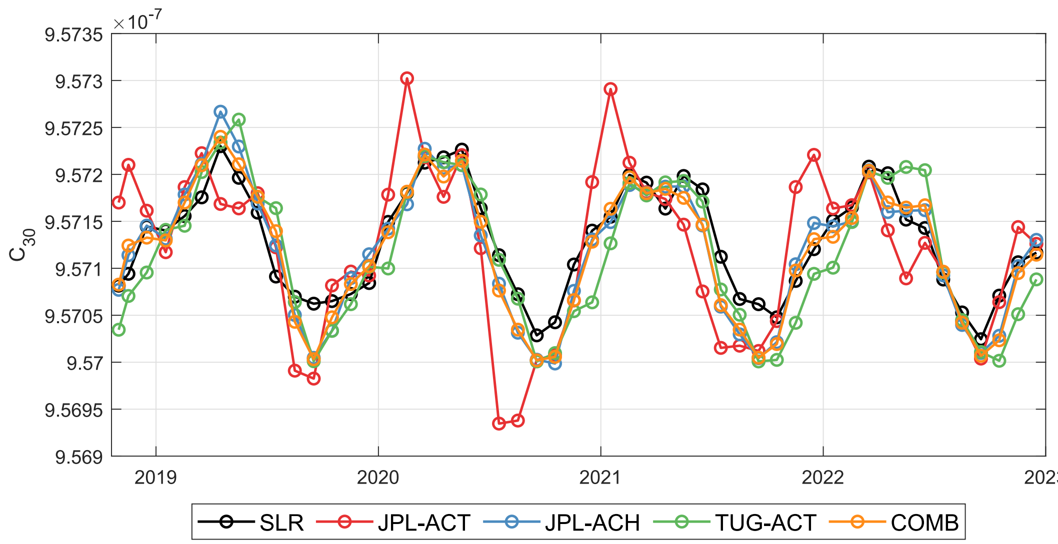

Figure 13. C_{30} estimates of Gravity Recovery and Climate Experiment Follow-on in four gravity field solutions. The satellite laser ranging values are given for reference.

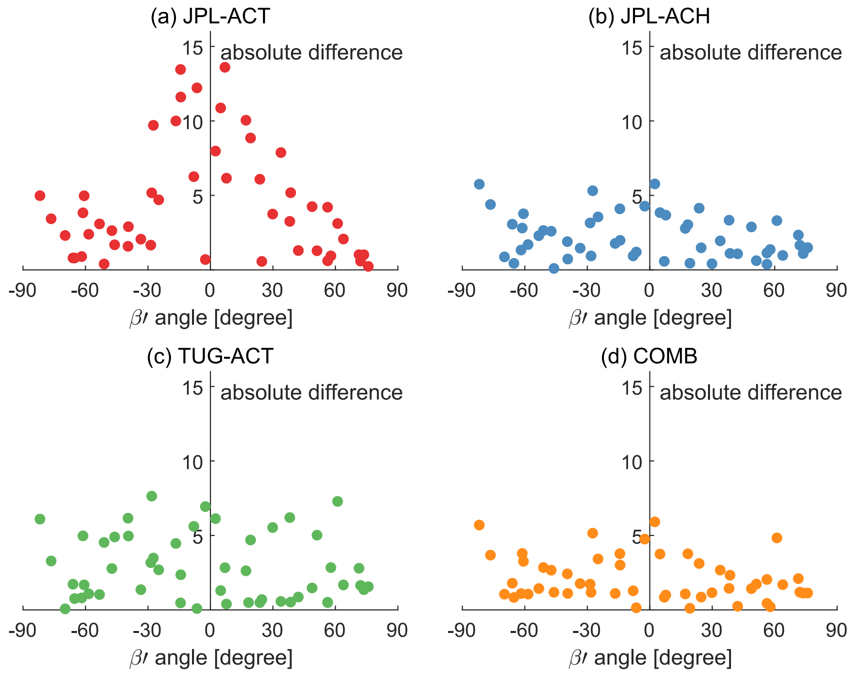

Figure 14. Absolute differences between C_{30} estimates from four Gravity Recovery and Climate Experiment Follow-on solutions and the satellite laser ranging in terms of β' angle. Note that the magnitude is scaled by 1×10^{11}.

highly consistent, and their differences from the reference are mostly limited to 2 mm, as shown in Figure S3 in Supporting Information S1. This also alleviates our concerns about potential contaminations to GRACE-FO science applications due to ACT product deficiencies, provided that reliable SLR estimates are available (Cheng & Ries, 2023; Loomis et al., 2019, 2020).

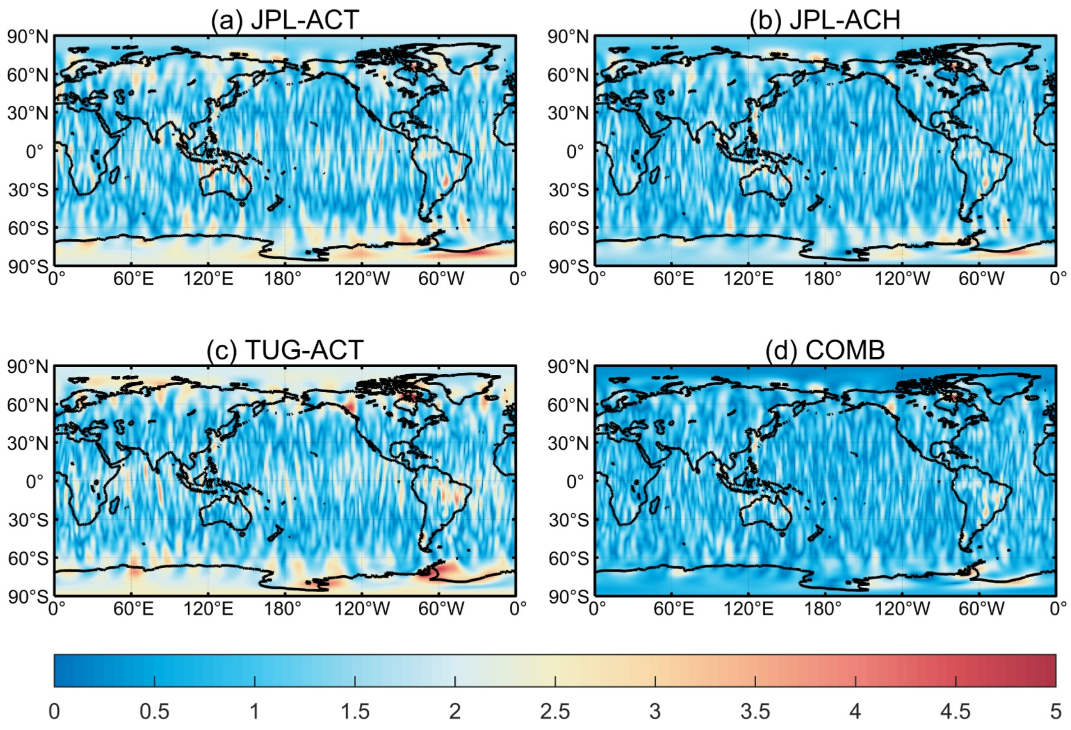

Figure 15. Amplitudes of the 161-day sinusoids in four gravity field solutions (unit: cm). C_{20} and C_{30} are from Gravity Recovery and Climate Experiment Follow-on estimates, and 300-km Gaussian smoothing is applied.

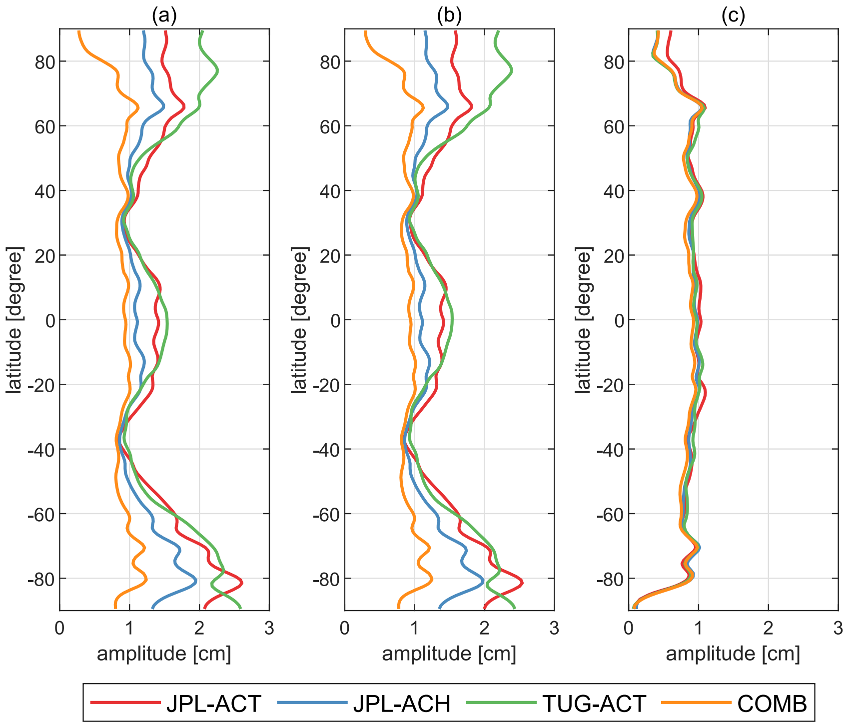

Figure 16. Average amplitudes of the 161-day signal for each latitudinal band in four gravity field solutions. 300-km Gaussian smoothing is applied. (a) C_{20} and C_{30} are from Gravity Recovery and Climate Experiment Follow-on (GRACE-FO) estimates. (b) C_{20} is from GRACE-FO, but C_{30} is replaced by satellite laser ranging (SLR). (c) Both C_{20} and C_{30} are replaced by SLR values.

3.4. Discussions on ACT Product Combination

The ACT product combination presented above is performed on the NEQ level as described in Section 2.2, while the direct combination of L1B-level accelerations is also feasible. Theoretically, both procedures should give consistent results since NEQ and L1B data contain the same information. Figure S4 in Supporting Information S1 compares gravity field solutions derived from either procedure, which confirms their agreement for most months.

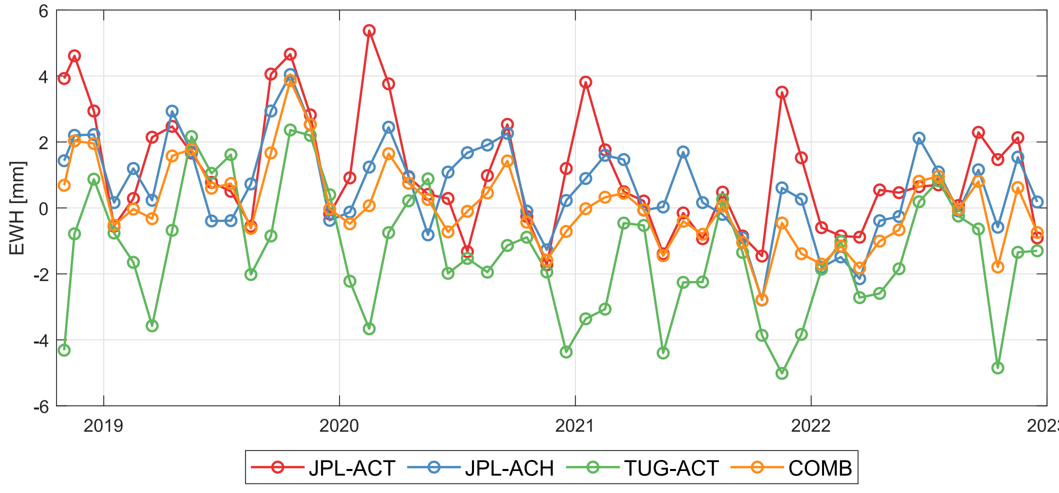

Figure 17. Differences in global mean ocean mass (GMOM) change estimates by four gravity field solutions with respect to the reference. The C_{20} and C_{30} are kept as their own estimates by Gravity Recovery and Climate Experiment Follow-on. The reference is defined as an ensemble average of three SDS solutions with C_{20} and C_{30} replaced by satellite laser ranging estimates. The GMOM change is given in terms of equivalent water height.

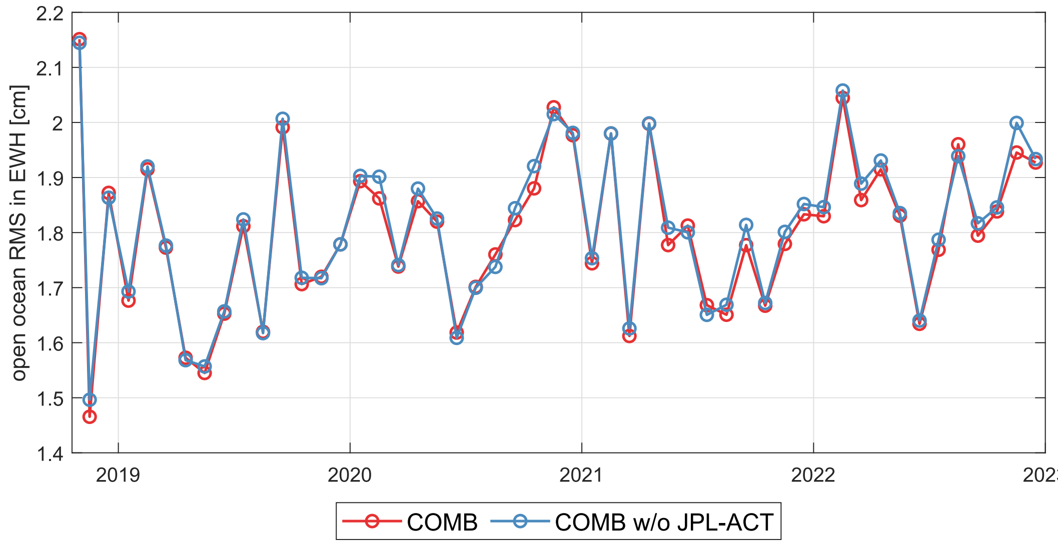

Figure 18. Monthly open ocean residuals root mean square (RMS) values of the combined solutions with and without JPL-ACT. Decorrelation filter and 300-km Gaussian smoothing are applied, and C_{20} and C_{30} are replaced by satellite laser ranging estimates.

Some noticeable discrepancies in the second half of 2021 and early 2022 are related to the nadir-pointing operation mode of the two GRACE-FO satellites and need further investigations. While it may be more efficient to process the weighted average of L1B data directly if their weights are known beforehand, we prefer to work on the NEQ level for tuning purposes, such as testing different weighting schemes. Changing weights in L1B-combination requires reintegrating satellite orbits and forming new normal equations for each time, which is the most time-consuming part of GRACE-FO L1B data processing. It can, however, be most easily and efficiently done at the NEQ level.

As the JPL-ACT will become outdated in future L1B data releases, it is important to assess the combination with only JPL-ACH and TUG-ACT. In Figure 18, we compare two versions of combined solutions, with and without JPL-ACT. The OOR values show almost negligible differences between the two, indicating that JPL-ACT provides little extra information in the combination. Additionally, Figures S5 and S6 in Supporting Information S1 display the time series of C_{20} and C_{30} estimates for both cases, along with SLR values. The RMS values of the differences between the SLR and the combined solution using only JPL-ACH and TUG-ACT are 7.2×10^{-11} and 2.7×10^{-11} for C_{20} and C_{30} estimates, respectively. These values are very close to those obtained using three ACT products, that is, the COMB in Table 3. The results indicate that the improvements resulting from the combined solution presented in previous sections are primarily attributed to the two advanced ACT products: TUG-ACT and JPL-ACH. This also confirms that the improvements are driven by enhanced non-gravitational force modeling via the combination rather than simply the accumulation of ACT data samples.

4. Summary and Conclusions

To address the GRACE-FO accelerometer issue, we comprehensively evaluate three operational ACT products, two from JPL (JPL-ACT and JPL-ACH) and one from TUG (TUG-ACT), using a consistent L1B data processing strategy, which serves as an independent and external validation in addition to the SDS team. Furthermore, we propose combining different ACT products to provide uniformly improved time series of monthly gravity field solutions by making the best of individuals. The combination is carried out by normal equations of gravity field models. Regarding the relative weights among individual normal equations in the combination, methods based on VCE and empirical noise estimation are compared and found to produce very similar combined solutions.

Four sets of monthly model series over the period October 2018 to December 2022 are produced using three different ACT products and their combination. Their qualities are evaluated in the spectral, temporal, and spatial domains with an emphasis on the noise level. The combined solution clearly improves SH coefficients of middleto-high degree and order, typically dominated by noise. Moreover, OOR, as a measure of noise level, indicate that the combined model series consistently achieves the lowest noise level for most months, which proves the strength of the ACT product combination. Compared to JPL-ACT, the noise reduction rates of JPL-ACH, TUG-ACT, and the combined model are 6%, 1%, and 12%, respectively, on average when 300-km Gaussian smoothing is applied. With different post-processing filters and C_{20} and C_{30} treatments, the average noise reduction rates of the combined solution are always the highest and are twice those of the second-best JPL-ACH. The combined solution is validated with the latest SDS solutions, further confirming its remarkably lower noise levels and their consistent signal contents.

As the quality of the ACT products significantly impacts the C_{20} and C_{30} estimates, we compare their values in different solutions with respect to the more reliable SLR-derived values. For C_{20}, the RMS of the differences between the SLR estimates and those of JPL-ACT, JPL-ACH, and TUG-ACT are 15.9×10^{-11}, 12.1×10^{-11}, and 14.9×10^{-11}, respectively, which indicates an improvement of JPL-ACH over its predecessor JPL-ACT as well as the TUG-ACT. The combined solution provides even better C_{20} estimates with an RMS value reduced to 7.6×10^{-11}, half that of JPL-ACH. This improvement greatly reduces the amplitudes of the 161-day spurious signal, which is most likely due to the combined effects of S2 ocean tide aliasing and accelerometer errors, with the latter dominating for GRACE-FO. For C_{30}, both JPL-ACH and TUG-ACT give more reliable estimates than JPL-ACT. Their RMS differences from SLR are 2.7×10^{-11} and 3.6×10^{-11}, respectively, while that of JPL-ACT is quite large at 6.2×10^{-11}. Again, the combined solution gives very close estimates to SLR with an RMS of 2.6×10^{-11}. Improvements in C_{20} and C_{30} estimates are directly translated into closer GMOM estimates to the reference, defined as an ensemble mean of three SDS estimates with C_{20} and C_{30} replaced by corresponding SLR values.

With the onset of the solar cycle 25, larger non-gravitational forces are expected due to increased solar activity, which demands an even more sophisticated technique of accelerometer data transplant. The previous assumption behind JPL-ACT that differences in non-gravitational forces between two satellites can be adequately handled by pure geometric corrections only may not hold well then; meanwhile, the remove-restore technique in TUG-ACT may reach its limit because of the expected increasing discrepancies between modeled and true non-gravitational forces in the context of intensifying solar activity. Therefore, before we can fully exploit the GRACE-D accelerometer, the hybrid ACT method in JPL-ACH that incorporates at least part of its real data should be preferred. In parallel, the ACT product combination strategy, as proposed in this study at the gravity field solution level, can be considered as a promising yet simple option at the moment. Furthermore, the combined use of only JPL-ACH and TUG-ACT yields results very close to those obtained using all three ACT products. This suggests that JPL-ACT provides minimal additional information and that only the two advanced ACT products (JPL-ACH and TUG-ACT) are necessary for the combination. In addition, the integration of different transplant techniques to create an even better ACT product will be a more convenient and advanced option in the future.

Acknowledgments

This study has been primarily supported by National Natural Science Foundation of China (42192532, 42174099, 42061134010, and 42394132) and Hong Kong RGC Collaborative Research Fund (C5013-23G). It also has received partial sponsorship from the Fundamental Research Funds for the Central Universities. Jianli Chen was supported by the PolyU SHS and LSGI Internal Research Funds (Project IDs: P0042322 & P0041486). The authors acknowledge the GRACE/GRACE-FO Science Data System for providing Level-1B science data, and also the Institute of Geodesy at Graz University of Technology for kinematic orbits and the ACT product. Yufeng Nie is grateful to Prof. Roland Pail for many fruitful discussions on GRACE/GRACE-FO gravity field recovery. The authors sincerely thank the reviewer and editors for their constructive comments, which help us to improve the manuscript.

Data Availability Statement

The GRACE-FO Level-1B data, including JPL-ACT and JPL-ACH, are available through: https://podaac.jpl.nasa.gov/dataset/GRACEFO_L1B_ASCII_GRAV_JPL_RL04. AOD1B RL06 models are from: https://podaac.jpl.nasa.gov/dataset/GRACE_AOD1B_GRAV_GFZ_RL06. GRACE-FO kinematic orbit data from TUG can be downloaded via: https://ftp.tugraz.at/outgoing/ITSG/satelliteOrbitProducts/operational/. TUG ACT product can be downloaded via: https://ftp.tugraz.at/outgoing/ITSG/GRACE/L1B/ACT1B/. C_{20} and C_{30} estimates by SLR in TN-14 can be accessed through: https://archive.podaac.earthdata.nasa.gov/podaac-ops-cumulus-docs/gracefo/open/docs/TN-14_C30_C20_GSFC_SLR.txt. The SDS GRACE-FO model series are available at: https://podaac.jpl.nasa.gov/dataset/GRACEFO_L2_CSR_MONTHLY_0062 for CSR RL06.2, https://podaac.jpl.nasa.gov/dataset/GRACEFO_L2_JPL_MONTHLY_0061 for JPL RL06.1, and https://podaac.jpl.nasa.gov/dataset/GRACEFO_L2_GFZ_MONTHLY_0061 for GFZ RL06.1.

References

Abrykosov, P., Sulzbach, R., Pail, R., Dobslaw, H., & Thomas, M. (2022). Treatment of ocean tide background model errors in the context of GRACE/GRACE-FO data processing. *Geophysical Journal International*, *228*(3), 1850–1865. https://doi.org/10.1093/gji/ggab421

Bandikova, T., McCullough, C., Kruizinga, G. L., Save, H., & Christophe, B. (2019). GRACE accelerometer data transplant. *Advances in Space Research*, *64*(3), 623–644. https://doi.org/10.1016/j.asr.2019.05.021

Behzadpour, S., Mayer-Gürr, T., & Krauss, S. (2021). GRACE follow-on accelerometer data recovery. *Journal of Geophysical Research: Solid Earth*, *126*(5). https://doi.org/10.1029/2020jb021297

Bettadpur, S., & McCullough, C. (2017). The classical variational approach. In M. Naeimi & J. Flury (Eds.), *Global gravity field modeling from satellite-to-satellite tracking data* (pp. 81–95). Springer. https://doi.org/10.1007/978-3-319-49941-3_3

Beutler, G., Jäggi, A., Hugentobler, U., & Mervart, L. (2006). Efficient satellite orbit modelling using pseudo-stochastic parameters. *Journal of Geodesy*, *80*(7), 353–372. https://doi.org/10.1007/s00190-006-0072-6

Beutler, G., Jäggi, A., Mervart, L., & Meyer, U. (2010). The celestial mechanics approach: Application to data of the GRACE mission. *Journal of Geodesy*, *84*(11), 661–681. https://doi.org/10.1007/s00190-010-0402-6

Brockmann, J. M., Schubert, T., & Schuh, W.-D. (2021). An improved model of the Earth's static gravity field solely derived from reprocessed GOCE data. *Surveys in Geophysics*, *42*(2), 277–316. https://doi.org/10.1007/s10712-020-09626-0

Cazenave, A., & Chen, J. (2010). Time-variable gravity from space and present-day mass redistribution in the Earth system. *Earth and Planetary Science Letters*, *298*(3–4), 263–274. https://doi.org/10.1016/j.epsl.2010.07.035

Chen, J. (2019). Satellite gravimetry and mass transport in the earth system. *Geodesy and Geodynamics*, *10*(5), 402–415. https://doi.org/10.1016/j.geog.2018.07.001

Chen, J., Cazenave, A., Dahle, C., Llovel, W., Panet, I., Pfeffer, J., & Moreira, L. (2022). Applications and challenges of GRACE and GRACE follow-on satellite gravimetry. *Surveys in Geophysics*. https://doi.org/10.1007/s10712-021-09685-x

Chen, J., Tapley, B., Tamisiea, M. E., Save, H., Wilson, C., Bettadpur, S., & Seo, K. W. (2021). Error assessment of GRACE and GRACE follow-on mass change. *Journal of Geophysical Research: Solid Earth*. https://doi.org/10.1029/2021jb022124

Chen, J., Tapley, B., Wilson, C., Cazenave, A., Seo, K. W., & Kim, J. S. (2020). Global ocean mass change from GRACE and GRACE follow-on and altimeter and Argo measurements. *Geophysical Research Letters*, *47*(22), e2020GL090656. https://doi.org/10.1029/2020GL090656

Chen, J. L., Wilson, C. R., & Seo, K.-W. (2008). S2 tide aliasing in GRACE time-variable gravity solutions. *Journal of Geodesy*, *83*(7), 679–687. https://doi.org/10.1007/s00190-008-0282-1

Chen, J. L., Wilson, C. R., & Tapley, B. D. (2010). The 2009 exceptional Amazon flood and interannual terrestrial water storage change observed by GRACE. *Water Resources Research*, *46*(12). https://doi.org/10.1029/2010wr009383

Chen, Q., Shen, Y., Chen, W., Francis, O., Zhang, X., Chen, Q., et al. (2019). An optimized short-arc approach: Methodology and application to develop refined time series of Tongji-Grace 2018 GRACE monthly solutions. *Journal of Geophysical Research: Solid Earth*, *124*(6), 6010–6038. https://doi.org/10.1029/2018jb016596

Chen, Q., Shen, Y., Kusche, J., Chen, W., Chen, T., & Zhang, X. (2020). High-Resolution GRACE monthly spherical harmonic solutions. *Journal of Geophysical Research: Solid Earth*, *126*(1). https://doi.org/10.1029/2019jb018892

Cheng, M., & Ries, J. (2017). The unexpected signal in GRACE estimates of C_{20}. *Journal of Geodesy*, *91*(8), 897–914. https://doi.org/10.1007/s00190-016-0995-5

Cheng, M., & Ries, J. (2023). C_{20} and C_{30} variations from SLR for GRACE/GRACE-FO science applications. *Journal of Geophysical Research: Solid Earth*, *128*(2), e2022JB025459. https://doi.org/10.1029/2022JB025459

Coddington, O., Lean, J. L., Pilewskie, P., Snow, M., & Lindholm, D. (2016). A solar irradiance climate data record. *Bulletin of the American Meteorological Society*, *97*(7), 1265–1282. https://doi.org/10.1175/bams-d-14-00265.1

Desai, S. D. (2002). Observing the pole tide with satellite altimetry. *Journal of Geophysical Research-Oceans*, *107*(C11). https://doi.org/10.1029/2001jc001224

Dobslaw, H., Bergmann-Wolf, I., Dill, R., Poropat, L., Thomas, M., Dahle, C., et al. (2017). A new high-resolution model of non-tidal atmosphere and ocean mass variability for de-aliasing of satellite gravity observations: AOD1B RL06. *Geophysical Journal International*, *211*(1), 263–269. https://doi.org/10.1093/gji/ggx302

Dow, J. M., Neilan, R. E., & Rizos, C. (2009). The international GNSS Service in a changing landscape of global navigation satellite systems. *Journal of Geodesy*, *83*(3–4), 191–198. https://doi.org/10.1007/s00190-008-0300-3

Flechtner, F., Save, H., Mccullough, C., Dahle, F. L., Bettadpur, S., Gaston, R., & Snopek, K. (2023). GRACE-FO: Science mission status and plans towards the extended mission phase. EGU General Assembly 2023, Vienna, Austria.

Ghobadi-Far, K., Werth, S., Shirzaei, M., Loomis, B. D., Döhne, T., Willen, M. O., & Horwath, M. (2023). The impact of new accelerometer transplant data (ACH) on GRACE follow-on along-orbit inter-satellite laser ranging observations and monthly time-variable gravity and mascon solutions. *Journal of Geophysical Research: Solid Earth*, *128*(6). https://doi.org/10.1029/2023jb026740

Han, S.-C., Shum, C. K., & Matsumoto, K. (2005). GRACE observations of M2 and S2 ocean tides underneath the Filchner-Ronne and Larsen ice shelves, Antarctica. *Geophysical Research Letters*, *32*(20). https://doi.org/10.1029/2005gl024296

Harvey, N., McCullough, C. M., & Save, H. (2022). Modeling GRACE-FO accelerometer data for the version 04 release. *Advances in Space Research*, *69*(3), 1393–1407. https://doi.org/10.1016/j.asr.2021.10.056

Jäggi, A., Meyer, U., Lasser, M., Jenny, B., Lopez, T., Flechtner, F., et al. (2020). International combination Service for time-variable gravity fields (COST-G). https://doi.org/10.1007/1345_2020_109

Jäggi, A., Weigelt, M., Flechtner, F., Güntner, A., Mayer-Gürr, T., Martinis, S., et al. (2019). European gravity service for improved emergency management (EGSIEM)—From concept to implementation. *Geophysical Journal International*, *218*(3), 1572–1590. https://doi.org/10.1093/gji/ggz238

Klinger, B., & Mayer-Gürr, T. (2016). The role of accelerometer data calibration within GRACE gravity field recovery: Results from ITSG-Grace 2016. *Advances in Space Research*, *58*(9), 1597–1609. https://doi.org/10.1016/j.asr.2016.08.007

Koch, K. R., & Kusche, J. (2002). Regularization of geopotential determination from satellite data by variance components. *Journal of Geodesy*, *76*(5), 259–268. https://doi.org/10.1007/s00190-002-0245-x

Kusche, J. (2003). A Monte-Carlo technique for weight estimation in satellite geodesy. *Journal of Geodesy*, *76*(11–12), 641–652. https://doi.org/10.1007/s00190-002-0302-5

Kvas, A., Behzadpour, S., Ellmer, M., Klinger, B., Strasser, S., Zehentner, N., & Mayer-Gürr, T. (2019). ITSG-Grace 2018: Overview and evaluation of a new GRACE-only gravity field time series. *Journal of Geophysical Research: Solid Earth*, *124*(8), 9332–9344. https://doi.org/10.1029/2019jb017415

Kvas, A., Brockmann, J. M., Krauss, S., Schubert, T., Gruber, T., Meyer, U., et al. (2021). GOCO06s – A satellite-only global gravity field model. *Earth System Science Data*, *13*(1), 99–118. https://doi.org/10.5194/essd-13-99-2021

Kvas, A., & Mayer-Gürr, T. (2019). GRACE gravity field recovery with background model uncertainties. *Journal of Geodesy*, *93*(12), 2543–2552. https://doi.org/10.1007/s00190-019-01314-1

Landerer, F., Flechtner, F., Save, H., McCullough, C., Dahle, C., Bettadpur, S., et al. (2022). Extending global mass change satellite observations into the third decade with GRACE-FO: Science mission status and plans. GRACE/GRACE-FO Science Team Meeting 2022, Potsdam, Germany.

Landerer, F. W., Flechtner, F. M., Save, H., Webb, F. H., Bandikova, T., Bertiger, W. I., et al. (2020). Extending the global mass change data record: GRACE follow-on instrument and science data performance. *Geophysical Research Letters*, *47*(12). https://doi.org/10.1029/2020gl088306

Lerch, F. J. (1991). Optimum data weighting and error calibration for estimation of gravitational parameters. *Bulletin Geodesique*, *65*(1), 44–52. https://doi.org/10.1007/bf00806341

Loomis, B. D., Rachlin, K. E., & Luthcke, S. B. (2019). Improved earth oblateness rate reveals increased ice sheet losses and mass-driven sea level rise. *Geophysical Research Letters*, *46*(12), 6910–6917. https://doi.org/10.1029/2019gl082929

Loomis, B. D., Rachlin, K. E., Wiese, D. N., Landerer, F. W., & Luthcke, S. B. (2020). Replacing GRACE/GRACE-FO with satellite laser ranging: Impacts on Antarctic ice sheet mass change. *Geophysical Research Letters*, *47*(3). https://doi.org/10.1029/2019gl085488

McCullough, C. M., Harvey, N., Save, H., & Bandikova, T. (2019). *Description of calibrated GRACE-FO accelerometer data products (ACT)*. NASA Jet Propulsion Laboratory, California Institute of Technology.

McCullough, C. M., Harvey, N., Save, H., Miller, M. A., Bertiger, W., Yuan, D.-N., & Landerer, F. W. (2022). Operational GRACE-FO accelerometer transplant strategies. AGU Fall Meeting 2022, Chicago, USA.

Meyer, U., Jäggi, A., Jean, Y., & Beutler, G. (2016). AIUB-RL02: An improved time-series of monthly gravity fields from GRACE data. *Geophysical Journal International*, *205*(2), 1196–1207. https://doi.org/10.1093/gji/ggw081

Meyer, U., Jean, Y., Kvas, A., Dahle, C., Lemoine, J. M., & Jäggi, A. (2019). Combination of GRACE monthly gravity fields on the normal equation level. *Journal of Geodesy*, *93*(9), 1645–1658. https://doi.org/10.1007/s00190-019-01274-6

Nie, Y., Shen, Y., Pail, R., & Chen, Q. (2022). Efficient variance component estimation for large-scale least-squares problems in satellite geodesy. *Journal of Geodesy*, *96*(2). https://doi.org/10.1007/s00190-022-01599-9

Nie, Y., Shen, Y., Pail, R., Chen, Q., & Xiao, Y. (2022a). Revisiting force model error modeling in GRACE gravity field recovery. *Surveys in Geophysics*. https://doi.org/10.1007/s10712-022-09701-8

Park, R. S., Folkner, W. M., Williams, J. G., & Boggs, D. H. (2021). The JPL planetary and lunar ephemerides DE440 and DE441. *The Astronomical Journal*, *161*(3). https://doi.org/10.3847/1538-3881/abd414

Peltier, W. R., Argus, D. F., & Drummond, R. (2018). Comment on "An assessment of the ICE-6G_C (VM5a) glacial isostatic adjustment model" by Purcell et al. *Journal of Geophysical Research: Solid Earth*, *123*(2), 2019–2028. https://doi.org/10.1002/2016JB013844

Petit, G., & Luzum, B. (2010). *IERS Conventions 2010*. Verlag des Bundesamts für Kartographie und Geodäsie.

Reigber, C. (1989). Gravity field recovery from satellite tracking data. In F. Sansò & R. Rummel (Eds.), *Theory of satellite geodesy and gravity field determination* (pp. 197–234). Springer Berlin. https://doi.org/10.1007/BFb0010552

Savcenko, R., & Bosch, W. (2012). EOT11a - empirical ocean tide model from multi-mission satellite altimetry. Deutsches Geodätisches Forschungsinstitut (DGFI), München, Germany.

Save, H., Bettadpur, S., & Tapley, B. D. (2012). Reducing errors in the GRACE gravity solutions using regularization. *Journal of Geodesy*, *86*(9), 695–711. https://doi.org/10.1007/s00190-012-0548-5

Scanlon, B. R., Zhang, Z., Save, H., Wiese, D. N., Landerer, F. W., Long, D., et al. (2016). Global evaluation of new GRACE mascon products for hydrologic applications. *Water Resources Research*, *52*(12), 9412–9429. https://doi.org/10.1002/2016WR019494

Scharroo, R., & Visser, P. (1998). Precise orbit determination and gravity field improvement for the ERS satellites. *Journal of Geophysical Research*, *103*(C4), 8113–8127. https://doi.org/10.1029/97jc03179

Seo, K. W., Wilson, C. R., Han, S. C., & Waliser, D. E. (2008). Gravity Recovery and Climate Experiment (GRACE) alias error from ocean tides. *Journal of Geophysical Research*, *113*(B3). https://doi.org/10.1029/2006jb004747

Suesser-Rechberger, B., Krauss, S., Strasser, S., & Mayer-Guerr, T. (2022). Improved precise kinematic LEO orbits based on the raw observation approach. *Advances in Space Research*, *69*(10), 3559–3570. https://doi.org/10.1016/j.asr.2022.03.014

Swenson, S., & Wahr, J. (2006). Post-processing removal of correlated errors in GRACE data. *Geophysical Research Letters*, *33*(8). https://doi.org/10.1029/2005gl025285

Tapley, B., Ries, J., Bettadpur, S., Chambers, D., Cheng, M., Condi, F., et al. (2005). GGM02 – An improved Earth gravity field model from GRACE. *Journal of Geodesy*, *79*(8), 467–478. https://doi.org/10.1007/s00190-005-0480-z

Tapley, B. D., Bettadpur, S., Ries, J. C., Thompson, P. F., & Watkins, M. M. (2004). GRACE measurements of mass variability in the Earth system. *Science*, *305*(5683), 503–505. https://doi.org/10.1126/science.1099192

Tapley, B. D., Watkins, M. M., Flechtner, F., Reigber, C., Bettadpur, S., Rodell, M., et al. (2019). Contributions of GRACE to understanding climate change. *Nature Climate Change*, *5*(5), 358–369. https://doi.org/10.1038/s41558-019-0456-2

Wahr, J., Molenaar, M., & Bryan, F. (1998). Time variability of the Earth's gravity field: Hydrological and oceanic effects and their possible detection using GRACE. *Journal of Geophysical Research*, *103*(B12), 30205–30229. https://doi.org/10.1029/98jb02844

Wouters, B., Bonin, J. A., Chambers, D. P., Riva, R. E., Sasgen, I., & Wahr, J. (2014). GRACE, time-varying gravity, Earth system dynamics and climate change. *Reports on Progress in Physics*, *77*(11), 116801. https://doi.org/10.1088/0034-4885/77/11/116801

Zehentner, N., & Mayer-Gürr, T. (2015). Precise orbit determination based on raw GPS measurements. *Journal of Geodesy*, *90*(3), 275–286. https://doi.org/10.1007/s00190-015-0872-7